

**RT SOLUTIONS, Inc.**

9 Channing Street, Cambridge, MA 02138.

Final Report  
O3MSAF-VS, 30 June 2010

**GOME-2 Trace Gas Column Retrievals:  
Optimized Wavelengths for the O<sub>3</sub> AMF**

**Robert J. D. Spurr<sup>(1)</sup>**

**Pieter Valks<sup>(2)</sup>, Nan Hao<sup>(2)</sup>, Diego Loyola<sup>(2)</sup>**

*<sup>(1)</sup>Director, RT Solutions, Inc.  
9 Channing Street, Cambridge, MA 02138*

*<sup>(2)</sup>German Aerospace Center (DLR)  
Remote Sensing Technology Institute (IMF)  
PO Box 1116, D-82234 Wessling, Germany*

30 June 2010

*Contractual Manager*

Seppo Hassinen  
Finnish Meteorological Institute,  
P.O.BOX 503, FIN-00101 Helsinki, Finland

# GOME-2 DOAS/AMF Algorithms: AMF Wavelengths

2

## 1. Introduction

GOME-2 on METOP-1 was launched on October 19 2006. GOME-2 has four linear array detectors; these four channels range from 240 to 800 nm with moderate resolution, and there are a number of polarization measurement devices. The current operational processing for total O<sub>3</sub> uses the GDP Version 4.4 DOAS algorithm. GOME-2 total ozone retrieval uses the GDOAS algorithm developed at BIRA-IASB and first used at DLR in 2004 as GDP Version 4.0 for the reprocessing of the GOME-1 total ozone record [Van Roozendael *et al.*, 2006; Balis *et al.*, 2007].

The DOAS least squares' fitting returns the O<sub>3</sub> slant column, effective temperature, polynomial closure parameters, amplitudes for Ring and under-sampling effects, and a shift factor compensating for wavelength registration effects. The AMF and VCD (vertical column density) calculations are done iteratively; there is a semi-empirical molecular Ring effect correction. Cloud information comes from the OCRA (cloud fraction) and ROCINN (cloud-top height and albedo) pre-processing steps. The fitting window is 325-335 nm, and AMFs are calculated at 325.5 nm. For details, see the GOME-2 ATBD [Valks *et al.*, 2010].

The GDP 4.4 algorithm for GOME-2 uses the same methodology, but there are some differences. These include the Level 1b calibration for GOME-2, and the choice of O<sub>3</sub> reference cross-sections. The biggest departures are the wider swath (960 km GOME-1, 1920 km GOME-2) and improved spatial resolution. GOME-2 views out to 63° from nadir; radiative transfer calculations must account for line-of-sight attenuation in a curved atmosphere. AMFs are calculated on the fly (no look-up tables) using the LIDORT 3.3 radiative transfer model [Spurr, 2008]; this has the line-of-sight path sphericity correction for the single scatter field.

The GOME-2 swath is twice that of GOME-1; the validations have shown a significant west-east scan angle bias in total O<sub>3</sub> and residuals. GOME-2 total ozone columns showed a bias of about +1.5-2% from the west to east ground-pixels [Balis *et al.*, 2009]; values of the bias were both spatial and temporally variable. Also, in the DOAS fitting, residuals for east pixels were found to be about 10% larger than west pixel residuals. This scan-angle dependency was not affected by subsequent use of GOME-2 level1B-R1 data (version 4.0). This dependency was also seen in comparisons with Dobson ground-based data.

A number of possible explanations have been sought for this phenomenon. A preliminary investigation at DLR using the vector radiative transfer model VLIDORT for the AMF calculations has shown that scan angle bias may be reduced by ~50% for low- and mid-latitudes; there was no clear improvement for higher latitudes. More recently, the focus has been on biases in the Level 1b data (R. Lang, EUMESAT, September 2009), perhaps caused by unresolved calibration issues, but at the time of writing the issue has not been resolved.

In the second half of 2009, an empirical or "soft" correction was introduced into the GDP 4.4 algorithm to deal with this bias [Loyola *et al.*, 2010]. For each forward scan angle, total ozone latitudinal monthly means were computed from two full years of GOME-2 data (2007 and 2008). All measurements were then normalized to reference values (zonal mean columns at the four west-most scan angle positions), and then given polynomial filtering to remove outliers. Smoothed correction factors depend on latitude and solar zenith angle, and are presented on a monthly basis. Figure 1 (taken from [Loyola *et al.*, 2010]) shows correction factors for GOME-2 total ozone values, plotted for two months according to scan angle and latitude, with values ranging from nearly 1.03 for some extreme east pixels (negative scan angles) to nearly 1.0 (no

# GOME-2 DOAS/AMF Algorithms: AMF Wavelengths

correction) for most pixels at the western end of the swath.

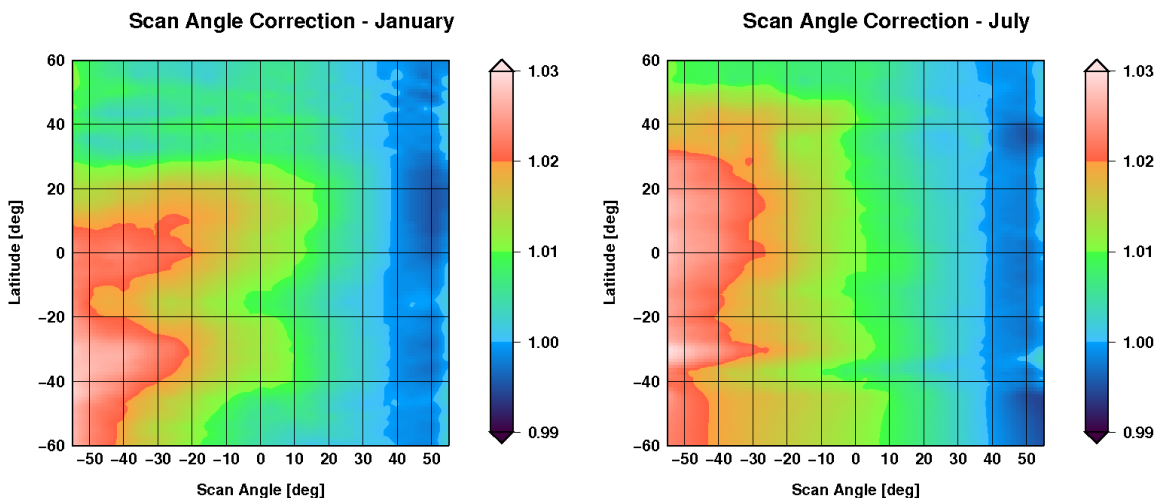


**Figure 1.** Correction factors for scan-angle bias in GOME-2 total ozone.

Aside from Level 1b calibration issues, there are several sources of uncertainty in the existing GDP 4.4 algorithm. In this report, we confine our attention to the issue of wavelength choices for the AMF computation. For all DOAS-style algorithms up to and including GDP 4.4, there has always been a fixed wavelength for ozone AMF computation.

For GOME-1, 325.0 nm was the original choice up to and including GDP 3.0. Using simulated GOME-1 radiances, it was found that total ozone errors of up to 5% are possible for SZAs > 80°, with generally 0.5-1% error for SZAs < 80° [van Roozendaal *et al.*, 2002]. These errors are reduced (to the 1-2% level for SZA > 80°) when 325.5 nm is used – this is the current value for GOME-1, and this is the default for GOME-2. Is the wavelength 325.5 nm for AMF computation the optimal choice?

Section 2 sets up a methodology for examining the choice of wavelength for ozone AMFs. For a given value of the total ozone, we generate a window of synthetic clear-sky radiances then use them in an effective DOAS fitting to establish a slant column amount and a "truth" AMF value. We then experiment with a number of wavelength choices and other parameterizations in a series of AMF calculations to find values closest to the truth AMF.

Section 3 presents some results from these numerical experiments. In summary, we have found that the choice of wavelength is weakly dependent on viewing geometry, but strongly dependent on solar zenith angle (SZA), total column amount and albedo. We have developed a parameterization of the optimum wavelength in terms of its value at SZA 87°, and we use this to examine the improvement in AMF compared with the current GDP 4.x default (which uses a value of 325.5 nm in all cases).

This work was funded through an O3MSAF 2009 Visiting Scientist Grant awarded to RT Solutions Inc., for the period 1 January 2009 through 30 September 2009 with an extension to 31 December 2009. This is the final report for this work.

## 2. Methodology for AMF wavelength study

### 2.1 Outline of the method

We expect that the choice of an optimum wavelength for the AMF calculation will depend on a number of quantities, including the solar and satellite geometry, the choice of ozone profile and the surface albedo. With this in mind, we create a "sandbox" for carrying out a theoretical study of the AMF wavelength optimization.

First, for a given set  $V$  of solar and viewing geometries, and given choices of ozone total column  $\Omega_{true}$  and albedo  $R$ , we use the VLIDORT radiative transfer model [Spurr, 2008] to create a set of synthetic clear sky sun-normalized radiances  $I(\lambda_i)$  at GOME-2 wavelengths  $\lambda_i$  inside the window 325-335 nm. [We use the TOMS V8 ozone climatology to establish the ozone column-profile link, see next section]. This window is the DOAS fitting choice in GDP 4.x; wavelengths are taken directly from a sample GOME-2 solar extra terrestrial measurement.

Second, for each such synthetic measurement characterized by geometry  $V$ , albedo  $R$ , and total ozone column and  $\Omega_{true}$ , we perform a single linear DOAS fit using a modified form of the Beer-Lambert relation with polynomial closure:

$$Y(\lambda_i) \equiv \ln[I(\lambda_i)] = -E\sigma_1(\lambda_i) - D\sigma_{12}(\lambda_i) - \sum_{j=0}^3 \alpha_j \left(1 - \frac{\lambda_i}{\lambda^*}\right)^j \quad (1)$$

Here,  $I(\lambda_i)$  is the synthetic spectrum,  $E$  the *effective* slant column density,  $\sigma_1(\lambda_i)$  is the associated ozone absorption cross section at temperature  $T_1$ ,  $D$  the difference slant column with reference spectrum  $\sigma_{12}(\lambda_i)$  equal to the difference between  $O_3$  cross-sections at temperatures  $T_1$  and  $T_2$ ). There are 4 closure parameters  $\alpha_j$ , and  $\lambda^*$  is a reference value set at 330 nm. We are ignoring fitting amplitudes for the Ring and under-sampling interference effects which are part of the operational fitting using real Level 1b spectra, and we also ignore non-linear shift-fitting associated with wavelength registration mismatches between solar and earthshine Level 1b data. Given fitted slant column  $E$ , the truth AMF is then specified according to

$$A_{true}(V, R, \Omega_{true}) = \frac{E}{\Omega_{true}}. \quad (2)$$

Third, we make a whole series of AMF calculations over a fine grid of wavelengths from 325 to 327.5 nm (at a resolution 0.01 nm), using the standard AMF definition:

$$A(\lambda) = \frac{\log(I_{nog}(\lambda)/I_g(\lambda))}{\tau_{vert}(\lambda)}. \quad (3)$$

Here  $I_g$  is the radiance for an atmosphere including ozone as an absorber, and  $I_{nog}$  is the radiance for an ozone-free atmosphere;  $\tau_{vert}$  is the vertical optical depth of ozone. VLIDORT is again used to do the radiative transfer for both these radiances, with simulations based on the same optical property setups as used in the synthetic spectrum computation in Step (1). We then find that wavelength  $\lambda(V, R, \Omega_{true})$  for which  $A(\lambda)$  is closest to  $A_{true}(V, R, \Omega_{true})$ .

Repeated application of these three steps will generate a data set of optimal wavelengths  $\{\lambda(V, R, \Omega_{true})\}$ . The fourth step is to examine ways in which this data set of wavelengths can be

# GOME-2 DOAS/AMF Algorithms: AMF Wavelengths

used in practice inside the GDP 4.x algorithm. It should be emphasized that GDP 4.x already has on-the-fly AMF calculations which are based on repeated upgrades of the vertical column amount. This iterative AMF technique was pioneered for GDP3 (which used neural network functions for AMF delivery); for a description in the GDP 4.0 context, see [Van Roozendael *et al.*, 2006]. We are not trying to supplant the existing AMF computations in GDP 4.x; merely, we wish to find a simple way of choosing an optimal wavelength without the need for an enormous and cumbersome additional look-up table.

**Remark.** This "effective fitting" methodology is akin to the AMF approach behind the DOAS algorithms used at KNMI to process Level 1b data from both the GOME instruments and also from SCIAMACHY and OMI. Here, a whole Look-up table data set of AMFs is established using the offline creation of synthetic radiances and the application of single DOAS fits. This LUT is then used to interpolate to the desired AMF value to be used in real-time retrievals of total ozone using proper Level 1b data.

## 2.2. Setups for VLIDORT simulations and DOAS Fittings

Ozone profiles are taken from the TOMS Version 8 climatology [Bhartia *et al.*, 2003], which is the default data set in GDP 4.x (all versions). This is a monthly column-classified data set divided into 18 latitude zones, with Umkehr profiles in Dobson Units specified for a number of total column amounts; for example in high latitudes, profiles are specified for columns 125 DU to 575 DU at 50 DU intervals. Profiles are given on an 11-layer pressure grid based on scale-height halving. The TOMS V8 also comes with temperature profile climatology on the same pressure grid and same latitude/month classification; this may be used in conjunction with the ozone data.

For columns not equal to one of the TOMs values, we use the profile-column linear map:

$$U_j(V) = \left( \frac{V - V^{(1)}}{V^{(2)} - V^{(1)}} \right) U_j^{(2)} + \left( \frac{V^{(2)} - V}{V^{(2)} - V^{(1)}} \right) U_j^{(1)}. \quad (4)$$

Here, we are given total column  $\Omega$ , and the associated profile  $\{U_j\}$  is expressed as a linear combination of two adjacent profiles  $\{U_j^{(1)}\}$  and  $\{U_j^{(2)}\}$  with TOMS V8 total column values  $\Omega^{(1)}$  and  $\Omega^{(2)}$  bracketing  $\Omega$ .

In this study, most simulations were done with a fixed 17-layer (18 levels) mid-latitude PTH (pressure/temperature/height) grid. This has a 1-2 km resolution in the troposphere (coarser at higher levels). TOMS cumulative Umkehr ozone values (based on the above 11-layer pressure grid present in the database) are interpolated on to this fixed 18-level pressure grid in order to assign ozone distributions.

Some simulations were done directly using pressure and temperature straight from the TOMS data and assigning height levels using the hydrostatic equation with an accurate integration to include the variation of gravity with altitude. This procedure is the default in the GODFIT algorithm [Spurr *et al.*, 2010]. Of particular interest here is the effect of the temperature field on the determination of optimal AMF wavelength.

We require the total overall optical properties  $\{\Delta_n, \omega_n, \beta_{in}\}$  in each layer  $n$ . These are the layer extinction optical depth, the total layer single scattering albedo and the total layer phase function

# GOME-2 DOAS/AMF Algorithms: AMF Wavelengths

6

expansion coefficients (scalar RT with no polarization). For a clear sky layer:

$$\Delta_n = U_n \alpha_n + A_n \sigma_{Ray} ; \quad \omega_n = \frac{A_n \sigma_{Ray}}{\Delta_n} \quad (5)$$

Here the layer trace gas amount is  $U_n$ , with trace absorption cross section  $\alpha_n$ ;  $A_n$  is the air density for Rayleigh cross-section  $\sigma_{Ray}$ . For Rayleigh scattering  $\beta_0 = 1$ , with  $\beta_2 = (1-\rho)/(2+\rho)$  in terms of depolarization ratio  $\rho$ . Values of  $\rho$  and  $\sigma_{Ray}$  are taken from [Bodhaine *et al.*, 1999] (this is the GDP 4.0 standard). We work with the TOMS 11-layer pressure and temperature grid. There are no aerosols, and we use a Lambertian surface throughout, with a selection of albedos ranging from 0.05 to 0.8.

A range of geometries has been selected for the study, we choose 10 solar zenith angles from 15° to 87° degrees, with 6 viewing zenith angles from 0° to 53° degrees (covering the swath extension), and 7 relative azimuth angles (between solar and viewing directions) from 0° to 180°.

In the DOAS fitting, we tried 3 and 4 closure parameters, and it was found that 4 closure variables gave more consistent results. The initial value of the first closure parameter is 1.0; the other closure parameters are initialized to zero before the fitting. Initial values of the effective slant column and difference column were set at 1000 DU and 25 DU respectively. Ozone cross-sections were taken from the GOME-1 flight model data [Burrows *et al.*, 1999] or from the Breon-Daumont-Malicet data set [Daumont *et al.*, 1992]. The latter data set uses a quadratic parameterization of the cross-section temperature dependence. We chose temperatures of 221 and 241 K for the fitting.

## 3. Results

### 3.1. Sandbox settings

Rather than present results for all months and latitude bands, we have divided the latitude bands into 5 zones. These are the high-latitude southern and northern zones (greater than latitudes 60 north and south), the mid-latitude southern and northern zones (30 to 60 degrees latitude) and the tropics (below 30N and 30S). This follows the TOMS Version 8 column classification, in which the high-latitude zones in all months have profiles specified at 10 column values from 125 to 575 DU, the mid latitude zones have profiles specified at 8 column values from 225 to 575 DU and the tropics have 4 column values from 225 to 375 DU. These column classifications are too coarse for our purposes, so we have used a somewhat finer step length for the columns; namely 21 values of W from 125 to 575 DU at intervals of 15 DU for the high and mid-latitude zones, and 9 values of W from 225 to 325 DU at intervals of 16.5 DU in the tropics.

The basis of all results is a comparison of the simulated AMFs in Eq. (3) with the true value Eq. (2). Initial results showed that the choice of optimal wavelength was weakly dependent on viewing zenith angle, and very weakly dependent on the azimuth choices. Unsurprisingly, the strongest geometrical dependency comes through the solar zenith angle. Figure 2 has two contour plots of the relative differences between the true and simulated AMFs, against solar zenith angle (x-axis) and simulation wavelength from 325 to 327.5 nm (y-axis). The 325.5 nm straight line is added for comparison - this is the GDP default. These figures apply to a particular sub-set of simulations at 0° azimuth averaged over all viewing zenith angles, for two scenarios in the tropical latitude band. The low ozone (225 DU), low albedo (5%) result is shown in the upper

# GOME-2 DOAS/AMF Algorithms: AMF Wavelengths

7

panel of Figure 2, the high ozone (325 DU), high albedo case (20%) in the lower panel.

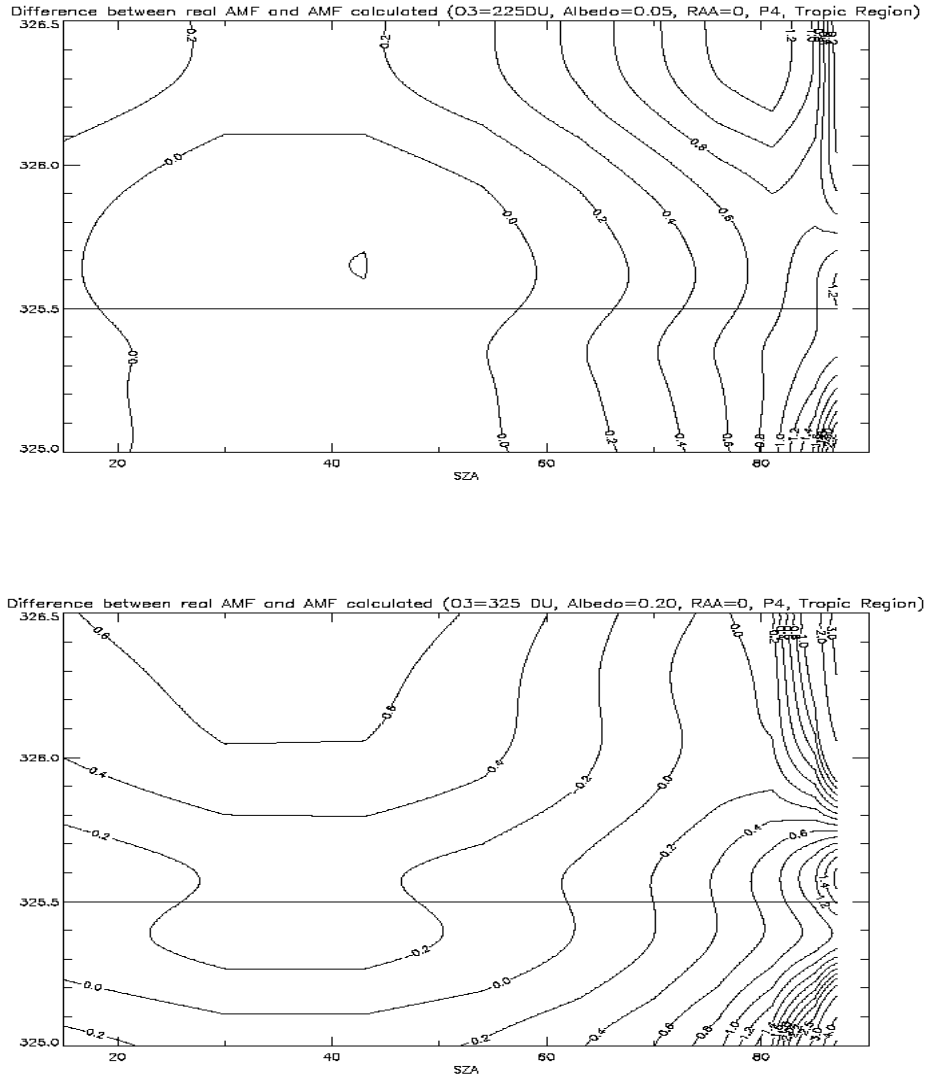


**Figure 2.** Contour plots of relative differences between simulated AMF values for various wavelengths, and the true AMF as determined in Eq. (2). The GDP default wavelength (325.5 nm) is marked by a straight line.

The contour pattern is broadly similar in both panels, and the same patterns have been observed in many other situations. In Figure 2, although the 325.5 nm default gives errors generally below 0.5% for low and moderate SZA values up to 60-65 degrees, it is increasingly inaccurate for higher SZA. In these plots, the optimal wavelength will follow the minimum error contour, and for higher solar zenith angles, this wavelength will increase above 325 nm to reach a maximum value at some SZA in excess of 80 degrees but not always at the highest value (87 degrees). This will be clear in the next section. Note that in the lower panel, there is some evidence of a double

# GOME-2 DOAS/AMF Algorithms: AMF Wavelengths

saddle at high SZA.

## 3.2. Examples of optimal wavelengths

In view of the weak viewing angle dependence, we have averaged all results over the 6 viewing angles ( $0^\circ, 13^\circ, 25^\circ, 35^\circ, 44^\circ, 53^\circ$ ) and 7 azimuth angles ( $0^\circ$  to  $180^\circ$  at  $30^\circ$  intervals). In the sequel, we use the notation  $\Lambda(\theta_0, R, \Omega_{true}) = \langle \Lambda(V, R, \Omega_{true}) \rangle$  to denote this geometrical averaging.

First, we examine a typical pattern for optimal wavelengths, in which values of  $\Lambda(\theta_0, R, \Omega_{true})$  are contour-plotted against solar zenith angle  $\theta_0$  and  $\Omega_{true}$  for the 5 latitude zones and for one albedo (0.05 in this case). In Figure 3, we show 10 contour plots of optimal wavelengths (on a scale from 325 to 327.5 nm as denoted by the color bars), arranged according to the 5 latitude zones from north to south (rows 1 through 5), and 2 time periods for January (left panels) and July (right panels). Figures on the y-axis are total columns  $\Omega_{true}$  (130 to 570 DU for mid-latitude and subarctic zones, and 230 to 320 DU for the tropics). The x-coordinate is SZA with values  $15^\circ, 30^\circ, 43^\circ, 54^\circ, 63^\circ, 70^\circ, 76^\circ, 81^\circ, 85^\circ$  and  $87^\circ$ .

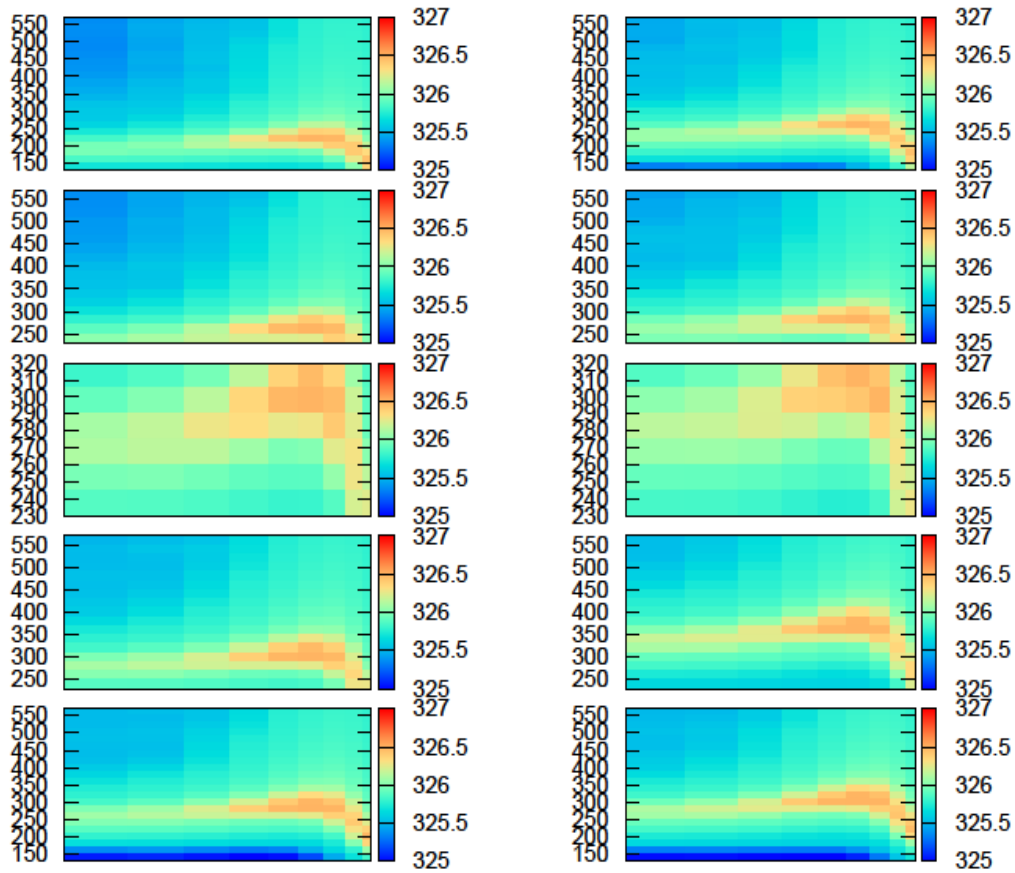


**Figure 3.** Contour plots of optimal AMF wavelengths for January (left panels) and July (right panels). The albedo is 0.05; five latitude zones are represented (see text for details).

## GOME-2 DOAS/AMF Algorithms: AMF Wavelengths

9

It will be seen that the optimal wavelength is only close to the default value 325.5 nm for low to moderate SZA angles and moderate to high amounts of total ozone. As with the contour plots in section 3.1, there is a slow increase with SZA in all cases, which suggests a linear parameterization would work in most cases (see next section). However there is a distinct surface of notably higher wavelengths which rises gradually with SZA up to  $\sim 70^\circ$ , then falls quite sharply with SZA. This curvature is similar in all the panels in Figure 2.

### 3.3. Linear parameterization of optimal wavelength

We look at a linear parameterization in terms of the value of the optical wavelength obtained at the highest SZA ( $87^\circ$ ). We set the optimal wavelength  $\Lambda_{15}$  at SZA  $15^\circ$  (the first value), and allow it to rise linearly with the cosine of the SZA until it reaches the value  $\Lambda_{87}$ . Thus the optimal wavelength as a function of SZA  $\theta_0$  is given by

$$\Lambda(\theta_0) = p \cos(\theta_0) + q, \quad (6)$$

with constants  $p$  and  $q$  defined for each zone and albedo by

$$p = \frac{\Lambda_{15} - \Lambda_{87}}{\cos 15^\circ - \cos 87^\circ}; \quad q = \Lambda_{87} - p \cos 87^\circ. \quad (7)$$

We take the same 5 latitudes, the same albedo, and this time we plot the relative errors between the true AMF and the computed AMF for two cases: (i) with the use of an optimal wavelength based on this  $\Lambda_{87}$  regression, and (ii) with the GDP 4.x default which uses a constant 325.5 nm wavelength for the AMF. Thus in Figure 4, we are plotting (left and right panels)

$$\varepsilon(\Lambda) = 100.0 * \left| 1 - \frac{AMF(\Lambda)}{AMF_{true}} \right|, \text{ where } \Lambda(\theta_0) = p \cos(\theta_0) + q \quad (8)$$

$$\varepsilon(\Lambda^*) = 100.0 * \left| 1 - \frac{AMF(\Lambda^*)}{AMF_{true}} \right|, \text{ where } \Lambda^* = 325.5 \text{ nm} \quad (9)$$

Figure 4 shows these errors for the month of January, again for all 5 latitude zones, and for a single albedo value of 0.05. The x- and y-axis classifications are the same as in the previous figure; the color-coding is the absolute relative error in %. On the left are AMF errors obtained using the linear regression (8), while on the right are errors based on use of the current GDP 4.x 325.5 nm default (9).

This figure gives a clearer indication of the improvement to be obtained in the AMFs using optimized wavelengths. A visual inspection shows that errors are smaller with the parameterized optimal wavelengths in all cases for the mid-latitude and tropical zones, with regression-induced errors no higher than 0.5% as opposed to values in excess of 2% with the 325.5 nm computations. However, the low ozone cases at high latitude are problematical, in that there does not appear to be a real improvement at higher SZA values with the atmosphere having 200 DU or less. This is especially the case in the southern hemisphere zone - the ozone hole scenario.

Figures 5 and 6 show the same plots for March and May, the patterns are similar, with some minor variations. Note again the lack of improvement in the low-ozone cases - we return to this point in the concluding remarks.

# GOME-2 DOAS/AMF Algorithms: AMF Wavelengths

10

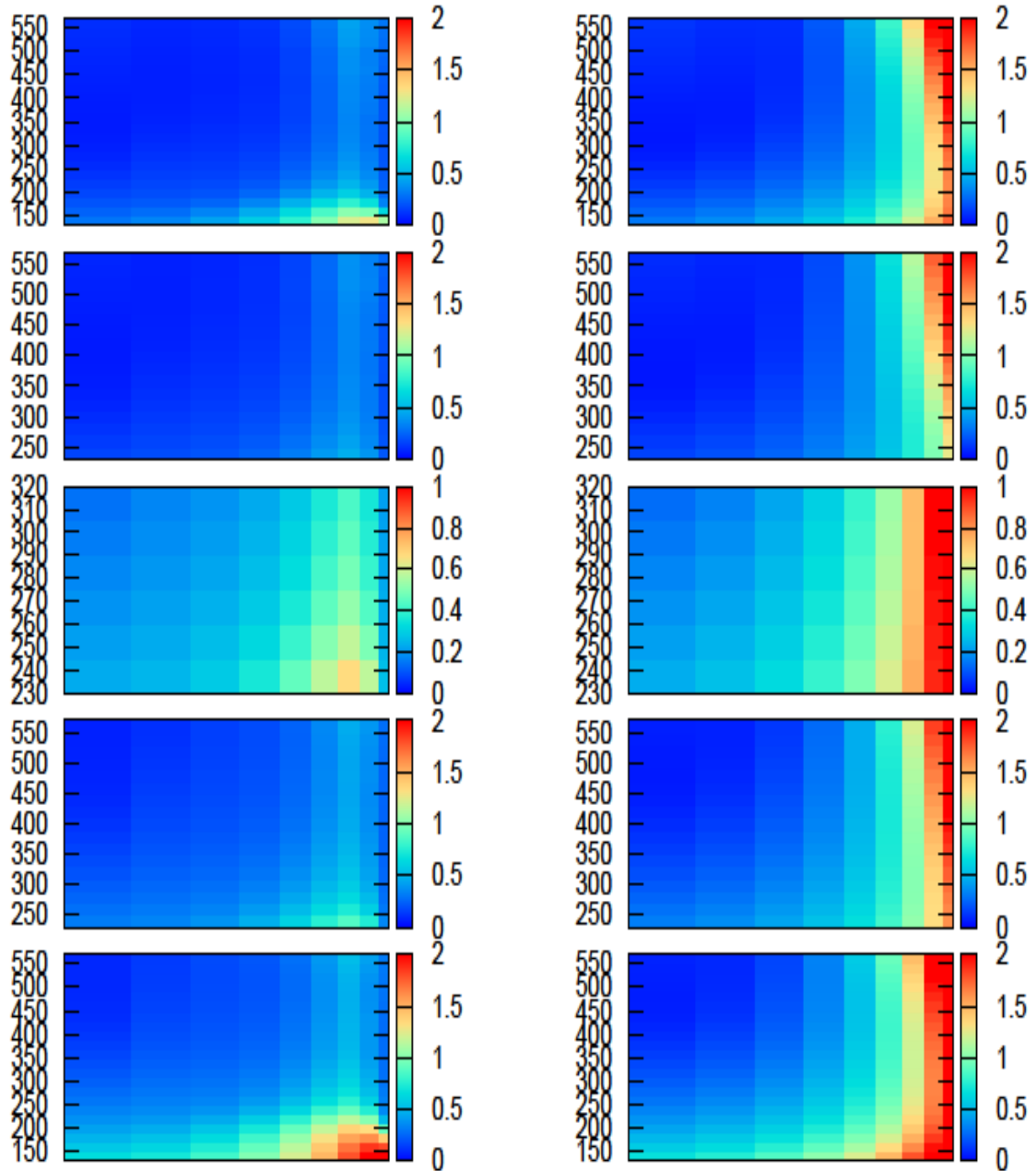


**Figure 4.** Contour plots of AMF errors when compared with the true AMF value. (Left panels) Using the SZA regression on optimal wavelengths; (right panels) using constant 325.5 nm for all AMF computation. January only; the albedo is 0.05; five latitude zones as in previous figure.

# GOME-2 DOAS/AMF Algorithms: AMF Wavelengths

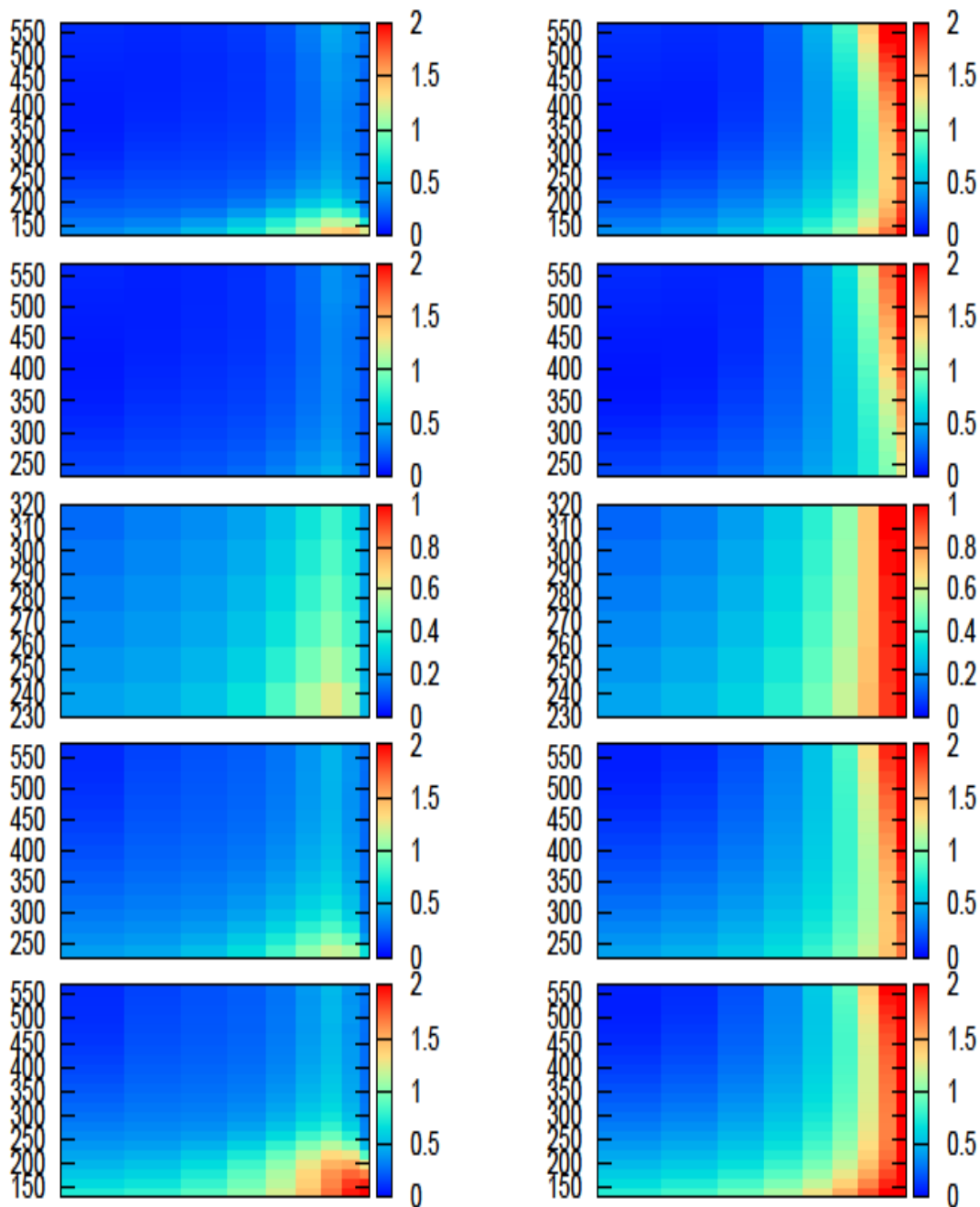


**Figure 5.** Contour plots of AMF errors when compared with the true AMF value. (Left panels) Using the SZA regression on optimal wavelengths; (right panels) using the constant 325.5 AMF computation wavelength. March only; the albedo is 0.05; five latitude zones as in previous figure.

# GOME-2 DOAS/AMF Algorithms: AMF Wavelengths

12

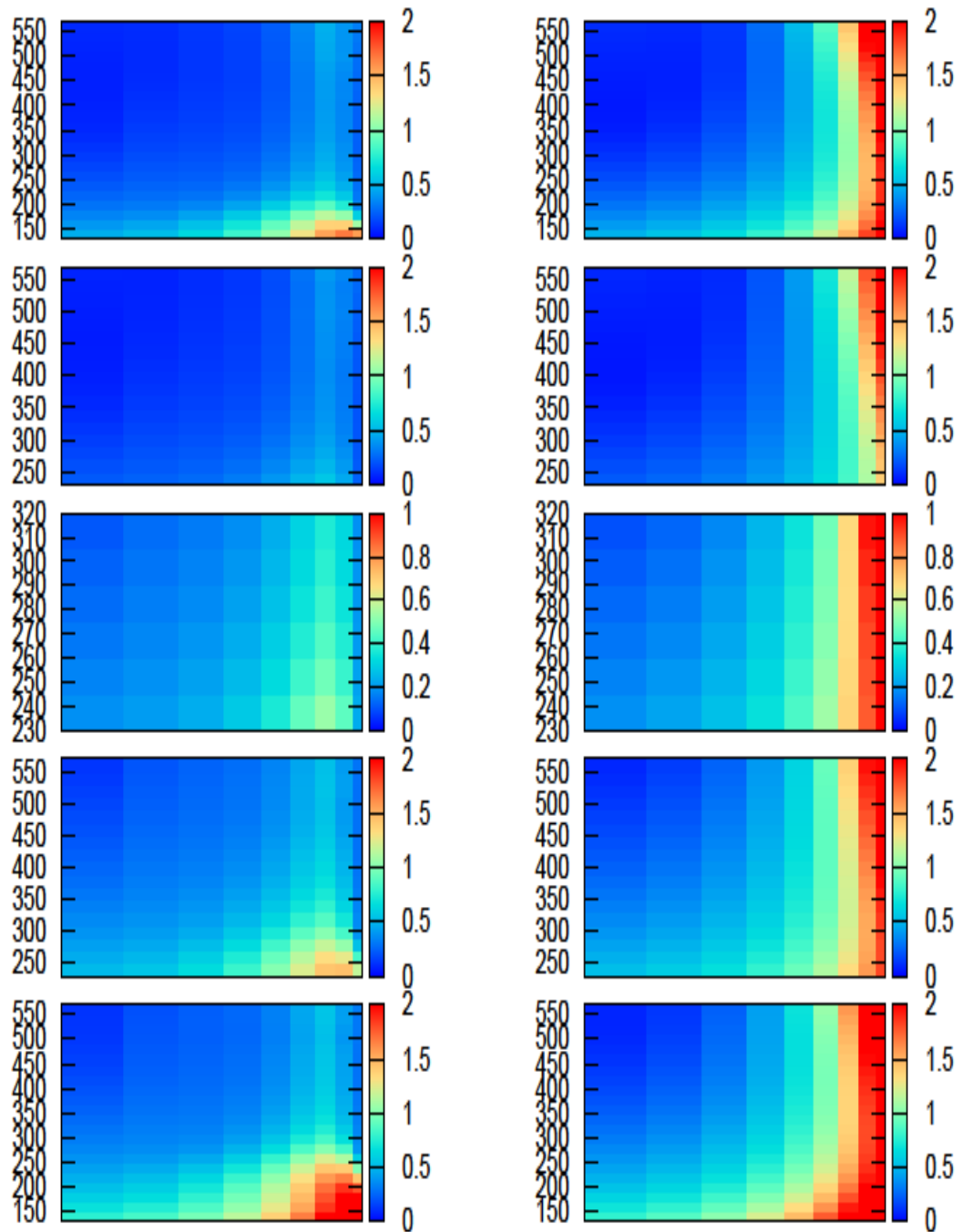
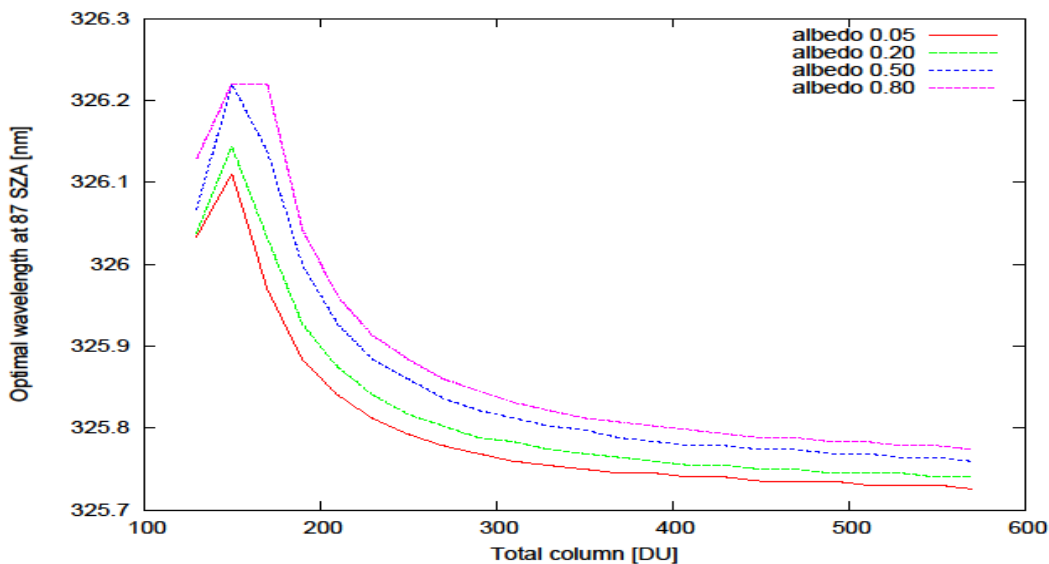


Figure 6. Similar to previous two figures. May only.

## 3.4. Albedo and other effects

It is clear from these figures that there is no simple way to improve the AMF result using a better guess for the wavelength of computation. Although there is a clear improvement in all cases looked at so far, there other physical considerations which complicate the picture.

First, we look at the effect of albedo. We have seen in Figure 4-6 that in some cases, there is little or no improvement for low total ozone scenarios. Figure 7 shows the optimal AMF wavelength at 87 SZA for the sub-arctic zone, plotted against the total ozone column, for 4 different values of the surface albedo as indicated. Behavior is smooth except for values of  $\Omega$  below 175 DU, where there is a trend reversal and some irregularities. In an operational context, one would have to rely on a look-up table to assign the optimal wavelength for AMF computation, with classifications according to discrete values of albedo and  $\Omega$ , and some interpolation scheme. The situation for  $\Omega > 175$  DU is smooth with similar curves and regular spacing. However it is difficult to imagine an LUT working satisfactorily in the depleted-ozone regime.



**Figure 7.** The averaged  $\Lambda_{87}$  optimal wavelength as a function of total ozone for 4 albedos as indicated; sub-arctic zone for the month of July.

In the next figure, we return to the tropical zone, this time looking at some complications due to forward model errors. In GDP 4.x, the AMF calculation is done using the scalar LIDORT model (no polarization), and this is the practice when calculating AMFs for comparison with the "true" value. However it is more correct physically to use synthetic spectra that have been computed with polarization included; a VLIDORT calculation for Stokes vector  $\mathbf{I} = \{I, Q, U\}$  (neglecting circular polarization) is needed here (the number of Stokes components NSTOKES=3). VLIDORT can of course be run in scalar mode (NSTOKES=1) to mimic the LIDORT result.

In Figure 8, results for 3 albedos are shown. The blue and green curves are based on the use of an

# GOME-2 DOAS/AMF Algorithms: AMF Wavelengths

14

11-layer atmospheric grid with temperature profile taken from the TOMS auxiliary temperature climatology that accompanies the ozone profile data; AMFs calculated for the optimized wavelength are always done in scalar RT mode (NSTOKES=1), but the "truth" AMF is obtained in two ways: with polarization (green curve), and without polarization (blue). Differences in these curves are not trivial.

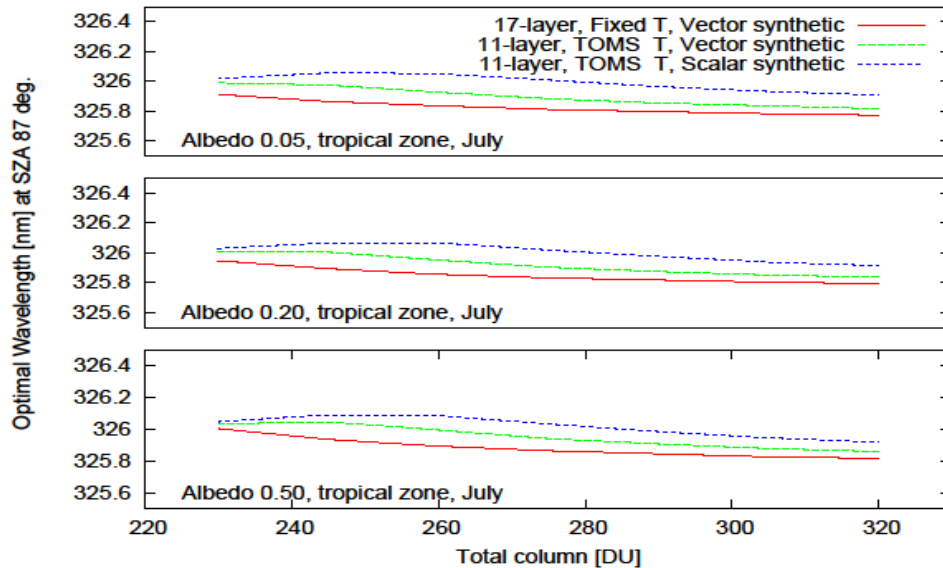


**Figure 8.** Averaged optimal wavelengths computed as a function of total ozone in the tropical zone, for 3 albedos: 0.05 (top), 0.20 (middle), 0.50 (lower panel). (Red curve) Simulations based on a fixed 17-layer grid with vector-RT synthetic spectra. (Green/blue curves) Simulations based on the 11-layer TOMS pressure grid, with and without polarization included in the synthetic spectra.

Also plotted in Figure 8 is the situation using a fixed-grid 17-layer atmosphere with given PTH (red curve), with the synthetic spectrum based on an RT computation including polarization. Apart from the finer gridding, the major effect here is the temperature profile (the 17-layer profile is for a midlatitude scenario). One could perform a whole raft of studies to investigate further the effects illustrated briefly here.

We confine our attention to examining the error patterns for two of these three curves. In Figure 9, the relative error between optimal-wavelength AMFs and the true AMF is shown for the tropical zone albedo choices in Figure 8. The left-hand panels show results using the 17-layer grid (corresponding to the red curve in Figure 8), the right hand panels are based on the 11-layer TOMS gridding (Green curve in Figure 8). In both cases, errors are below 1% for SZA < 80°, but results are marginally worse for the TOMS case; something of a paradox since this is supposed to have the "correct" temperature. It should be stated that these results are to taken with some caution, since under nominal operating conditions, GOME-2 SZA values in the 30N-30S

# GOME-2 DOAS/AMF Algorithms: AMF Wavelengths

15

geographical range do not reach to 80°, so that the choice of temperature profile is not so relevant.

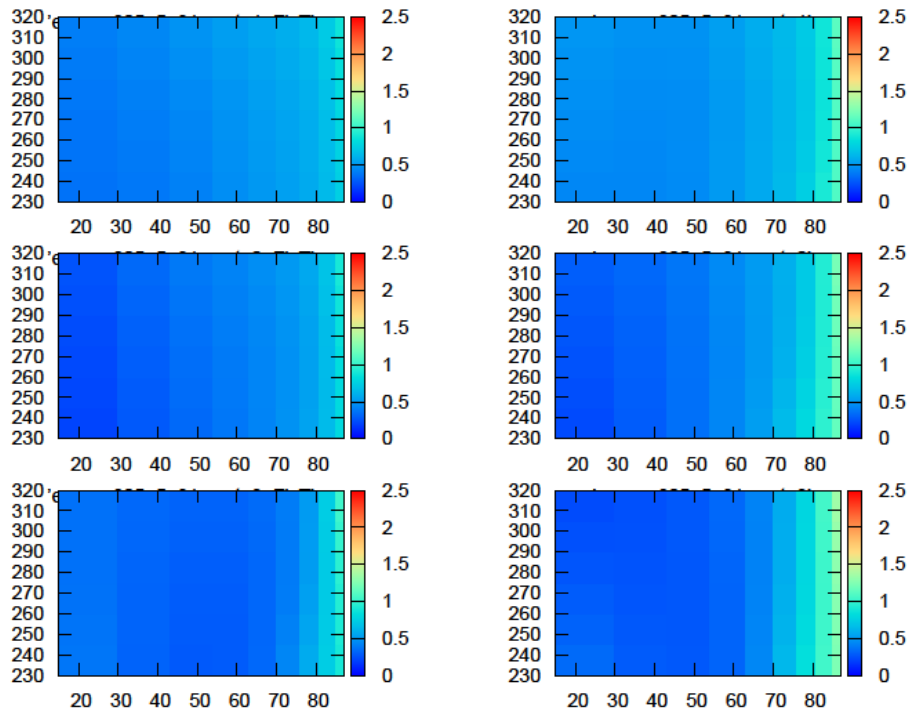


**Figure 9.** AMF error patterns for a fixed 17-layer grid (left) and for the 11-layer TOMS case (right); tropical ozone column values, 3 albedos as in Figure 8. SZA values (in degrees) on the x-axes, and total ozone in DU for the y-axes.

## 4. Concluding Remarks

Although it has been possible with this AMF tool to obtain a large number of results, it has proved difficult to find consistent patterns in these results, and to obtain workable parameterizations of the optimal wavelength choice that can be deployed in an operational DOAS-style total ozone retrieval algorithm. This is the case for clear-sky simulations; further work on partially cloudy and fully cloudy scenarios would merely introduce more layers of complexity.

Based on the results presented above and the classification schemes chose for this study, a look-up table of optimal wavelength regression coefficients was introduced in the GDP GOME-2 total ozone algorithm. Simulation of clear and cloudy-sky AMFs are based on the interpolated value of optimal wavelength selected from this LUT. Although it was found that the scheme was robust and for the most part delivered total ozone results that were in very good agreement with default values obtained with the 325.5 nm fixed-wavelength AMF assumption, there were instances with significant unexplained differences (up to 6%).

It should be remembered that DOAS retrieval for ozone relies on a number of physical

# GOME-2 DOAS/AMF Algorithms: AMF Wavelengths

16

assumptions that are marginally justified for a fitting window in a strongly scattering and absorbing part of the UV spectrum. It is conceivable that remote-sensing results for DOAS ozone have reached the limit of accuracy - the 1% level ([Balis *et al.*, 2007]). The next-generation GDP5 algorithm premiering for GOME-1 in 2010 is based on the proper simulation of backscattered radiance in the UV Huggins' bands, without the need for the two-step "slant-column-and-AMF-division" DOAS methodology based on Beer's law. To attempt another somewhat ad hoc AMF correction is perhaps "one bridge too far".

To demonstrate real improvements in DOAS-retrieved total ozone from LUT tables for AMF optimal wavelength, one would need to carry out an extensive validation exercise against ground-based network data and results from other satellites, as well as existing GDP 4.x products. Such an exercise is outside the scope of the present work, and would require a much greater resource investment. And even before such a validation exercise can take place, it would be necessary to devote further time and resources to examining this issue. In view of the foregoing remarks, it has been decided to conclude this investigation for now.

## References

- Balis D., M. Koukouli, D. Loyola, P. Valks, and N. Hao, Third O3MSAF Validation Report, SAF/O3M/AUTH/GOME-2VAL/RP/03, November 2009  
[http://atmos.caf.dlr.de/GOME-2/docs/AUTH\\_GOME-2\\_O3\\_VAL.pdf](http://atmos.caf.dlr.de/GOME-2/docs/AUTH_GOME-2_O3_VAL.pdf)
- Bhartia, P., Algorithm Theoretical Baseline Document, TOMS v8 Total ozone algorithm ([http://toms.gsfc.nasa.gov/version8/version8\\_update.html](http://toms.gsfc.nasa.gov/version8/version8_update.html)), 2003.
- Bodhaine, B., N. Wood, E. Dutton, and J. Slusser, On Rayleigh optical depth calculations, *J. Atmos. Ocean. Tech.*, **16**, 1854-1861, 1999.
- Burrows, J., A. Richter, A. Dehn, B. Deters, S. Himmelmann, S. Voigt and J. Orphal, Atmospheric remote-sensing reference data from GOME: Part 2. Temperature-dependent absorption cross-sections of O<sub>3</sub> in the 231-794 nm range, *J. Quant. Spectrosc. Radiat. Transfer*, **61**, 509-517, 1999.
- Deaumont, M., J. Brion, J. Charbonnier and J. Malicet, Ozone UV Spectroscopy I: Absorption cross-sections at room temperature, *J. Atmos. Chem.*, **15**, 145-155, 1992.
- Loyola, D. G., M. E. Koukouli, P. Valks, D. S. Balis, N. Hao, M. Van Roozendael, R. J. D. Spurr, W. Zimmer, S. Kiemle, C. Lerot, J.-C. Lambert, The GOME-2 Total Column Ozone Product: Retrieval Algorithm and Ground-Based Validation, submitted, *J. Geophys. Res.*, 2010.
- Spurr, R., LIDORT and VLIDORT: Linearized pseudo-spherical scalar and vector discrete ordinate radiative transfer models for use in remote sensing retrieval problems, *Light Scattering Reviews*, Volume 3, ed. A. Kokhanovsky, Springer, 2008.
- Valks P., D. Loyola, N. Hao, et al., Algorithm Theoretical Basis Document for GOME Total Column Products of Ozone, NO<sub>2</sub>, SO<sub>2</sub>, BrO, H<sub>2</sub>O, tropospheric NO<sub>2</sub>, Cloud Properties, DLR/GOME/ATBD/01, Iss./Rev. 2/C, 2010, [http://atmos.caf.dlr.de/gome2/docs/DLR\\_GOME-2\\_ATBD.pdf](http://atmos.caf.dlr.de/gome2/docs/DLR_GOME-2_ATBD.pdf)
- Van Roozendael M., V. Soebijanta, C. Fayt, and J.-C. Lambert, Investigation of DOAS Issues Affecting the Accuracy of the GDP Version 3.0 Total Ozone Product, in ERS-2 GOME GDP 3.0 Implementation and Delta Validation, Ed. J.-C. Lambert, ERSE-DTEX-EOD-TN-02-0006, ESA/ESRIN, Frascati, Italy, Chap.6, pp.97-129, 2002.
- Van Roozendael, M., D. Loyola, R. Spurr, D. Balis, J.-C. Lambert, Y. Livschitz, P. Valks, T. Ruppert, P. Kenter, C. Fayt, and C. Zehner, Ten years of GOME/ERS2 total ozone data: the new GOME Data Processor (GDP) Version 4: I. Algorithm Description, *J. Geophys. Res.*, doi: 10.1029/2005JD006375 (2006).